Appl. Phys. A (2014) 116:529–543
DOI 10.1007/s00339-014-8467-3

Applied Physics A
Materials Science & Processing

Structural and compositional modification of a barium boroaluminosilicate glass surface by thermal poling

Nicholas J. Smith · Carlo G. Pantano

Received: 27 March 2014 / Accepted: 21 April 2014 / Published online: 15 May 2014

Abstract In addition to inducing second-order nonlinear properties, significant structural and compositional alteration can be imparted to glass surfaces during the process of thermal poling. In this work, we focus on how thermal poling affects a structurally complex, nominally alkali-free boroaluminosilicate display glass composition. We provide evidence for electrolysis of the glass network, characterized by the migration of both cations (Ba^{2+}, Na^{+}) and anions (O^{-}, F^{-}) towards opposing electrode interfaces. This process results in oxidation of the positively biased electrode and forms a network-former rich, modifier-depleted glass surface layer adjacent to the anodic interface. The modified glass layer thickness is qualitatively correlated to the oxidation resistance of the electrode material, while extrinsic ions such as H^{+}/H_3O^{+} at not found in the depletion layer to compensate for the migration of modifier cations out of the region. Rather, FTIR spectroscopy suggests a local restructuring of the B_2O_3–Al_2O_3–SiO_2 network species to accommodate the charge imbalance created by the exodus of network-modifying cations, specifically the conversion of tetrahedral B(4) to trigonal B(3) as Ba or Na ions are removed from B-related sites in the parent network. The resultant poling-induced depletion layer exhibits enhanced hydrolytic resistance under acidic conditions, and the IR spectra are substantially unlike those produced by acid leaching the same glass.

N. J. Smith · C. G. Pantano (✉)
Department of Material Science and Engineering, Materials Research Institute, The Pennsylvania State University, University Park, PA 16802, USA
e-mail: cgp1@psu.edu

Present Address:
N. J. Smith
Science and Technology Division, Corning Incorporated, Corning, NY, USA

1 Introduction

The process of thermal poling—comprised of modest thermal treatment in combination with an applied electric field—provides a method for achieving substantial and lasting modification of glass surfaces and has been studied significantly in recent years primarily for creating second-order nonlinearity (SON) [1, 2]. However, it has also been recognized that such treatments—when performed with suitable, ion-blocking electrodes—can yield nanoscale glass surface layers of modified composition [3–8], analogous to the modified interfacial layers which develop during anodic bonding of a metallic or semiconducting electrode materials to glass [9–11]. The compositional modification is typically characterized by a depletion of mobile cations in the high-field region near the positively biased electrode (i.e. the anode), such that a space-charge polarization is set up that can be quenched into the glass to provide SON.

From a glass science perspective, a key question that arises from these observed phenomena is exactly how the atomic structure of the glass accommodates the observed compositional changes that occur during poling. As mobile cations are induced to migrate, the fate of anionic sites within the glass structure—species such as non-bridging oxygen (NBO) and $[AlO_4]^{-}$ or $[BO_4]^{-}$ tetrahedra—must be considered when rationalizing the final structure of the glassy, network-former-rich, depletion layer. In the absence of protons or other counter-ions, local coordination changes and condensation reactions can be expected to rearrange the "parent" glass structure to maintain the

charge-balance requirements of the network-forming elements.

The existence of oxygen-anion transport and the resultant transformation of the original glass structure have been reported previously in poled glasses. One of the earliest was shown by Carlson and collaborators [7, 8, 12], revealing the viability of electrolytic surface modification in simple alkali silicates to create a network-former-rich layer—essentially SiO_2. In those glasses, the only anions within the "parent" network were NBO species, which upon poling, resulted in a more connected SiO_2 network and gaseous O_2 evolution. Dussauze and collaborators have reported on many similar observations for poling of soda-lime glass and alkali phosphates, with evidence for enhanced network connectivity in the network-former-rich layers using vibrational spectroscopy, as well as evidence for the liberation of molecular species at the anode [3, 4, 6, 13]. A comparable effect has been reported by Baucke and Duffy in studies of alkali-rich borates [14, 15], though in this instance the parent glass possessed a more complex initial structure due to the presence of both 3- and 4-coordinated B units (the latter charge-compensated by alkali) comprising the backbone of the structure. In the anodic bonding literature, extensive evidence for depletion layers with attendant interfacial oxidation has been observed in bonding of alkali silicates and borosilicate glasses [9, 16–18], as well as alkali-free boroaluminosilicate glass, to single-crystal silicon [10], implying oxygen release and structural modification. Polarization studies of the interfacial layers have confirmed an irreversible, charge-neutral layer [11, 19], while quantitative measures of the residual electric field in the poled layer consistently suggests fields at or below the intrinsic breakdown strength of the network [20]. These observations are both consistent with electrolysis of the network acting as a discharge mechanism during poling.

For this study, we focus on how the composition and structure is modified within the anodic surface layer of a model multicomponent glass with complex initial structure: a quaternary barium boroaluminosilicate glass (Schott AF45). This glass is differentiated from those used in most prior studies for two reasons. First, they are alkali-free, and thus present the opportunity to mobilize divalent Ba ions; and second, because they have very few NBO's in the parent structure, and instead comprise a mix of tetrahedral aluminum and boron anionic units. In terms of practical relevance, glasses in the $RO\text{-}B_2O_3\text{-}Al_2O_3\text{-}SiO_2$ family are noted for use as flat panel display substrates [21] and are also candidates for next-generation energy storage applications due to remarkably high dielectric breakdown strengths and energy densities [22–26]. The thermal poling characteristics of such glasses have been recently characterized in terms of the induced second-order nonlinearity [20].

1.1 Review of glass structure

Before examining the experimental results, it is helpful to briefly review the structural characteristics of the barium boroaluminosilicate (Ba-BAS) glass used in this study. This material has a molar bulk composition of 12 $\%BaO{\cdot}15\ \%B_2O_3{\cdot}9\ \%Al_2O_3{\cdot}63\ \%SiO_2$. Like other silicates, the structure can be envisioned from the starting point of a fully corner-shared $[SiO_4]$ tetrahedral network. The addition of BaO—a network modifier—to form a binary glass network would serve to reduce its connectivity, forming 2 NBO for every mole of BaO, with the cation present in the structure as a weakly bound species in close association with these NBO's for charge-compensation. When Al_2O_3 is added to this structure, it exhibits a strong preference to enter the silicate network in tetrahedral coordination. Due to the +3 valence state of Al, these 4-coordinated Al species also require charge-compensation. As a result, Ba^{2+} ions that would otherwise serve to form NBO are instead used to compensate the $[AlO_4]^-$ units (in equimolar proportions $BaO{:}Al_2O_3$). A similar mechanism is active with the addition of B_2O_3 to form $[BO_4]^-$ units, but the Al is modifier-compensated in preference to B. Any remaining B enters the network as 3-coordinated trigonal $[BO_3]$ units, while NBO on B only forms in the presence of substantial excess modifier.

In the final analysis for this particular glass—considering the species involved and their molar proportions in the bulk composition—it is assumed that the majority of available BaO modifier will be preferentially consumed, first for charge-compensating tetrahedral $[AlO_4]^-$ sites, with a very small minority of higher coordinated $[AlO_5]^-$ sites, and the remainder going to charge-compensate tetrahedral $[BO_4]^-$sites, with little to no NBO formation. A summary of the expected network structural units is depicted in Fig. 1. The preferential partitioning of modifier to Al over B in boroaluminosilicate systems has been well established [27–32], and the subsequent conversion of B to 4-coordinated state with the remaining Ba is most valid at relatively low fractions of excess modifier and high Si/(B+Al) ratios [29, 33, 34]. This has been found to be particularly true when the field strength of the cation is relatively low, as is the case with barium [35, 36]. Thus, the Ba in this composition is expected to be associated with the B and Al anionic units, and not to form NBO, as corroborated in comparable glasses [37]. The specific structural roles of the minority species, including a low (0.19 at %) concentration of arsenic (As) as a fining agent, as well as impurity-level species such as sodium (Na), water (H_2O), and fluorine (F), are not significant in determining the network structure.

The predominance of the large divalent modifier Ba^{2+}, and the fact that it is modifying the local environment of

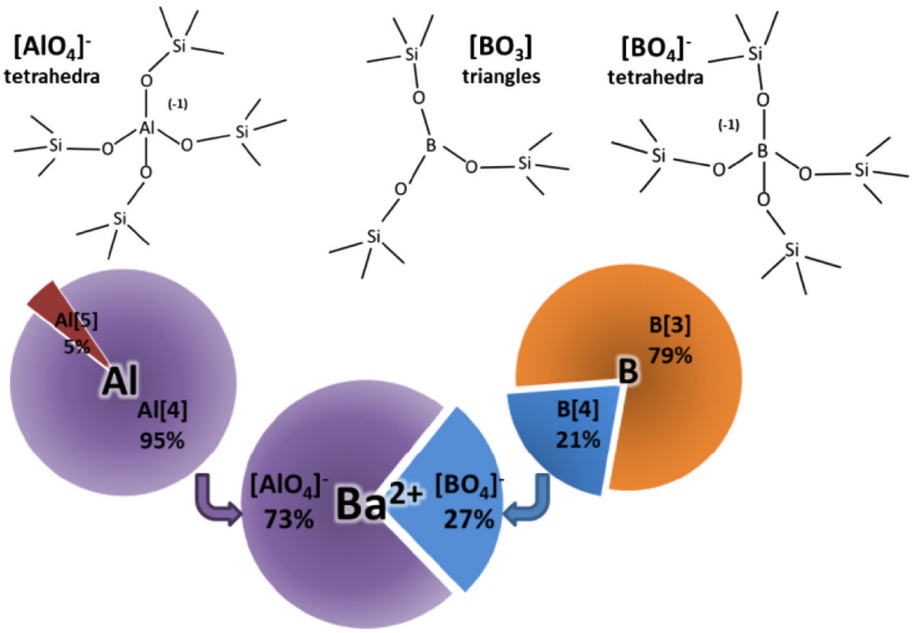

Fig. 1 Schematic depiction of Al and B-containing structural units in the parent glass structure and their corresponding consumption of Ba modifier (in preference of NBO formation)

anionic Al and B network formers, provides an interesting and unique scenario for this high-temperature thermal poling study. Evidence is provided for electrolysis of the glass network, characterized by the migration of both cations (Ba^{2+}, Na^{+}) and anions (O^{-}, F^{-}) towards opposing interfaces. This process results in oxidation of the positively biased electrode along with formation of a nanoscale cation-depleted layer adjacent to the anodic interface composed of only the network-forming elements—in this case, a cation-B_2O_3-Al_2O_3-SiO_2 glass. The cation-depleted layer thickness is qualitatively correlated to the oxidation resistance of the electrode material. Through SIMS depth-profiling, a minimal contribution from extrinsic ions such as H^{+}/H_3O^{+} is confirmed, which along with FTIR spectroscopy of the modifier depleted layer implicates network structure changes in the response of the glass to thermal poling. In a complementary report [38], we describe the speciation of aluminum in the depleted layer, using Al K-edge XANES as an element-specific probe for local structural modifications around these sites which further support the findings reported in this paper.

2 Experimental procedure

The samples in this study were a nominally alkali-free barium boroaluminosilicate (Ba-BAS) glass, Schott AF45 (Schott Technologies Inc.). Its approximate molar bulk composition is 63 % SiO_2·12 % BaO·15 % B_2O_3·9 % Al_2O_3 plus minor components (0.19 % As_2O_3 as a fining agent) and trace-level impurities including ~440 ppma Na. Glass samples were either 0.4 or 1 mm thick.

Poling treatments were performed at temperatures ranging from 300 to 600 °C—all below the 627 °C strain point for this glass—and poling times were held constant at 30 min throughout this study. All processing was performed in high vacuum ($0.5–3.0 \times 10^{-6}$ torr) inside a tube furnace to minimize the injection of positive charge-carrying species from the atmosphere (e.g. H^{+}) at the anode interface. The temperature of the sample was monitored directly with a thermocouple in intimate contact with the cathode side of the glass sample. Samples were equilibrated at the requisite poling temperature until the desired working pressure was achieved prior to poling. Poling voltages in the range of 2–6 kV were applied using a high-voltage supply (Model 610C; Trek). Voltages were applied in an instant-on fashion. For this work, press-contact electrodes were employed to facilitate removal of the electrode without complex etching steps, thereby preserving the modified surface for analysis. Electrodes ($\sim 1 \times 2''$) of either Pt or PtSi films (on Si) were used as anode-contact materials, while either sputter-deposited Pt films or high-purity carbon foil was used as cathode-contact material. At the conclusion of poling, most samples could be separated from the electrodes with minor mechanical force, indicating a weak anodic bonding effect. None of the poling resulted in dielectric breakdown.

After separation, confocal micro-Raman spectroscopy aided in the evaluation and identification of phases formed at the electrode-glass interface. Unpolarized Raman spectra were collected in back-scatter geometry with 488 nm Ar-ion laser excitation on a WiTec CRM200 confocal spectrometer equipped with a thermoelectrically cooled CCD detector and a 100X (N.A. = 0.9) objective. Spectra were

acquired using either 600 or 1,800 lines/mm diffraction gratings and integration times of 10–20 s.

Surface compositions and depth profiles of poled glass samples were obtained using X-ray photoelectron spectroscopy (XPS) performed on a Kratos Axis Analytical Ultra equipped with a monochromatic Al K_α (1,486.6 eV) X-ray source. To minimize potential effects of surface charging, a low-energy electron flood gun was directed at the surfaces during all spectral acquisitions. Initial survey scans were typically conducted over the range of 1,350–0 eV in 0.5–1.0 eV steps at 80 eV pass energy and 150–350 ms dwell time. High-resolution surface scans were performed at 20 eV pass energy for extended dwell times over narrow binding energy ranges corresponding to the elemental peaks in question. Since this Ba-BAS glass contained a significant concentration of both barium and boron, an overlap between the Ba4p and B1s photoelectron peaks was present that complicated direct analyses of composition. An empirical curve-fitting method was, therefore, developed to deconvolute the spectra in this region [39]. XPS data were quantified using CASA-XPS software, and surface compositions were subsequently corrected for the presence of any adventitious carbon overlayer using the method proposed by Smith [40]. For vacuum-poled glass samples, the apparent concentration of adventitious carbon was generally quite low at 1–5 atom % indicating a minimal influence of this correction, while as-received samples generally had typical apparent concentrations of 8–13 % of surface carbon.

In addition to surface analyses, sputter depth profiles were also performed in the XPS system, wherein samples were sputtered in 10–100 s cycles with 4 keV Ar^+ ions rastered over a 2 × 2 mm area to access successive in-depth regions. After each sputter cycle, spectra were acquired over narrow binding energy ranges at 80 eV pass energy using a ~200-mm diameter X-ray beam centered within the sputter crater. The average sputtering rate in this configuration was ~0.11 nm/s, as determined by optical profilometer measurements of sputter craters subsequent to profiling. The sputter rate was assumed to be constant and was used to determine an approximate depth scale for the XPS profiles. Since XPS is insensitive to hydrogen, a check for the role of H in poled depletion layers was also pursued by secondary-ion mass spectroscopy (SIMS) depth profiles of select samples at a separate facility (Evans Analytical Group; East Windsor, NJ). Analyses were conducted on a quadrupole SIMS specially designed for interrogation of insulating samples, with highly optimized charge compensation and acquisition procedures employed to minimize the diffusion of mobile species (e.g. H, Na) toward or away from the surface during analysis [41]. Hydrogen concentrations were calibrated against H in a SiO_2 film standard as determined by hydrogen forward-scattering (HFS) spectrometry. The quantification methodology has an absolute error bar of ±10 % since that is the uncertainty in the HFS measurement; however, the relative error between successive measurements is specified much lower at ~3 % and is the more appropriate uncertainty in discussing comparative data (as in the case of H in poled vs. unpoled glass).

Fourier-transform infrared reflectance spectroscopy (FTIRRS) was used to evaluate the poling-induced changes in glass structure. Measurements were conducted on a Bruker Hyperion 3,000 micro-FTIR system equipped with a high-performance MCT (HgCdTe) detector. Reflectance spectra were obtained in the mid-IR range of 4,000–580 cm^{-1} using a 15X infrared microscope objective focused on a clean analytical area of approximately 100 × 100 μm, as delineated using a set of knife-edge apertures. The effective angle of incidence for the objective was in the range of 20°–30° from vertical—sufficiently near-normal so as to discount any potential polarization effects. Spectra were acquired for multiple spots per sample in 200-scan passes at 2 cm^{-1} resolution, and a gold mirror was used as a standard reference for all measurements. The same surfaces were also evaluated by attenuated total reflectance (ATR) IR measurements. Spectra acquired in this mode exhibit surface sensitivity similar to reflectance measurements, but produce spectra more directly analogous to absorbance measurements. These spectra were acquired using a nitrogen-purged single-bounce diamond ATR accessory (MVP-Pro; Harrick) and a Bruker IFS-66 spectrometer system with a DTGS detector in 200-scan passes at 6 cm^{-1} resolution. To facilitate spectral comparison, data were normalized to an approximately uniform penetration depth by multiplying by υ/1,000, where υ = wavenumber (cm^{-1}).

3 Results

3.1 Depletion layer formation, composition and electrode effects

Figure 2 presents the measured extent of Ba depletion on the anode-side glass surfaces as a function of poling temperature. This datum is overlaid with the dependence of the second-order nonlinear coefficient on the same samples from quantitative Maker fringe analysis detailed in a separate report [20]. Examination of the figure shows that $\chi^{(2)}$ in the poled samples is maximized at approximately 450 °C, and the Ba concentration is essentially constant and equivalent to the as-received surface on thermal poling up to this temperature. At these temperatures, instead, an accumulation of Na was detected on the cathode surface, which indicated that Na was the primary mobile species

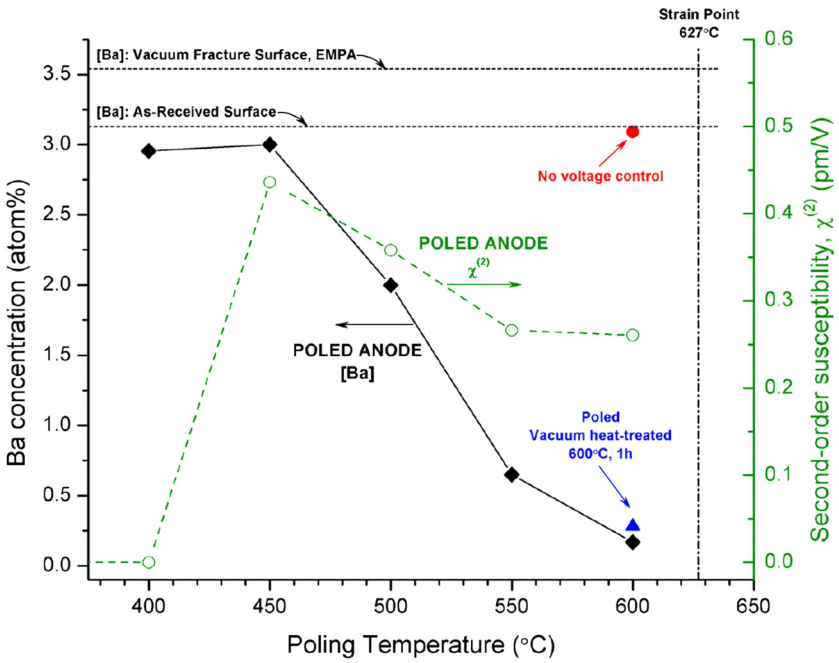

Fig. 2 Barium concentration (*closed symbols*) on poled anode-side surfaces of Ba-BAS glass as a function of poling temperature, as compared to reference/control samples. The corresponding second-order nonlinear coefficients, for samples poled in vacuum with Pt film electrodes ($V_{pole} = 4$ kV, $t_{pole} = 30$ min) as reported in [20], are also shown

responsible for second-order nonlinear (SON) activity. However, as the poling temperature is increased, the concentration of Ba at the anode surface begins to decrease. Thus, the activated drift of Ba^{2+} in this system correlates well with the decrease in $\chi^{(2)}$, the latter of which is generally attributed to the blocking condition being compromised at the anode and the subsequent compensation of charge in the network. The barium concentration continues to decrease with higher poling temperatures and for poling up to 600 °C, a minimum value of ~0.2 atom % Ba is observed at the surface. For the data in Fig. 2, we also plot the XPS surface composition of a "no-voltage" control sample: this sample was similarly press-contacted with a Pt film electrode and identically heat-treated in vacuum, the only difference being the absence of an applied voltage. This confirms that the poling-induced Ba depletion was not a result of spontaneous thermochemical (redox) effects that can also take place at a glass-to-metal interface. This conclusion is further verified by experiments with a reducing heat-treatment in forming gas at the glass' strain point. As this glass contains a small percentage of arsenic as a chemical fining agent, an inherent oxygen source arises via the reduction reaction $As_2O_5 \rightarrow As_2O_3 + O_2$. Such redox reactions can lead to interfacial oxidation and induce spontaneous inward diffusion of modifier species, reportedly even with low-mobility alkaline-earth species [42]. However, within a presumed 10 % error of XPS quantification, no discernible effect of such heat-treatments on the surface composition of this glass or electrodes was observed. Thus, it may be safely concluded that the induced compositional changes were a genuine result of poling. Another comparative data point is also provided in Fig. 2 to show that the depletion of Ba from the surface was unchanged after a 1-hour vacuum heat-treatment at the 600 °C poling temperature, confirming the formation of a stable/irreversible depletion layer at the surface. Select samples were also evaluated by X-ray diffraction and were found to be X-ray amorphous.

Summarized in Table 1 are the surface composition results for the poled-anode surfaces, where it is shown that in addition to the decrease in Ba, an accumulation of fluorine is also observed at the positively biased interface. The native F concentration in the bulk glass was estimated at <500 ppm-wt according to best estimates from electron microprobe analyses, and its distinct, upward trend with poling temperature indicates the migration of this anionic species from within the glass toward the positively biased electrode during the poling process. As for oxygen anions, Fig. 3 provides evidence for the transport and reaction of oxygen species to the Pt film electrode surface, observed after its separation from the glass. The inset image shows that the originally pristine metal surface took on a whitish, corroded appearance in the regions in contact with the glass during the poling process; all other regions not in contact with the glass retained the original metallic appearance of the Pt film. The visual severity of the corrosion qualitatively increased with increasing poling temperature. Subsequent analysis of the electrode surface by Raman spectroscopy confirmed the nature of the interfacial modification as being due to oxidation of the Pt. In the Raman spectra of Fig. 3, Pt metal shows no first-order Raman vibrations in this frequency range; thus the as-deposited Pt

Table 1 Surface composition as a function of temperature for various treatments, including samples poled with Pt film electrodes at different temperatures

	Surface composition by XPS (atom %)					
	O	Si	B	Al	Ba	F
As-Received	65.1	20.8	5.7	5.3	3.1	–
Vacuum H.T.[a] (in contact with Pt film)	64.4	21.1	6.1	5.3	3.1	–
Reducing H.T.[b]	64.6	21.9	5.3	5.3	2.9	–
Reducing H.T.[b] plus Vacuum H.T.[1] (in contact with Pt/Si)	64.6	22.1	5.1	5.4	2.9	–
Poled[c], 400 °C	65.1	21.1	5.8	5.0	3.0	–
Poled, 450 °C	65.1	20.3	6.1	5.1	3.0	0.3
Poled, 500 °C	63.4	21.0	6.2	5.2	2.0	2.3
Poled, 550 °C	63.2	21.6	7.2	4.6	0.7	2.8
Poled, 600 °C	62.9	21.6	7.6	4.2	0.2	3.5

[a] Heat treated at 600 °C in 0.5–3 × 10^{-6} torr for 2 h

[b] Heat treated in forming gas (5 % H_2/95 % N_2) at strain point (627 °C) for 2 h

[c] Poled with Pt film electrodes at 4 kV for 30 min

film exhibits a featureless spectrum (Fig. 3a) which is unaffected by vacuum heat-treatment alone at 600 °C (Fig. 3b). Used as a poling electrode, regions of the film not in contact with the glass were unaltered (Fig. 3c), while the region in contact with the glass during poling—and exhibiting the corroded appearance—showed a strong series of sharp peaks in the 300–800 cm^{-1} region. The inset spectra of Fig. 3 unambiguously assign the peaks to a platinum oxide phase, identified by Graham as Pt_5O_{6-} [43]. Altogether, the combined results provide evidence for migration of both cations (Ba^{2+}, Na^{+}) and anions (O^{-}, F^{-}) towards opposing electrode interfaces on poling of this glass at high temperatures.

An even more dramatic example of barium depletion and concomitant interfacial oxidation is observed with the use of an alternate electrode material that is more readily oxidized—specifically, PtSi. Oxidation of these electrodes was observed in the regions contacting the glass—and only with an applied voltage—by XPS and provided further evidence for oxygen anions migrating from the glass during poling. Unlike the case of Pt metal, the oxidation reaction with PtSi induced the formation of a SiO_2 layer at the interface instead of a Pt-oxide phase. This interfacial SiO_2 layer was found to be more strongly bonded to the glass surface than to the PtSi electrode, and upon separation of the glass sample from the electrode, it detached from the electrode to leave a thin SiO_2-rich "skin" on the poled glass surface that was not part of the original glass. A schematic depiction of this process is shown in Fig. 4a, along with XPS depth profile data illustrating the presence of the two different layers; this mechanism was further validated by optical profilometry, showing height-steps at the periphery of the poled region. But the main point here is the substantial Ba-depletion depths, which were thicker with PtSi than with Pt film electrodes. The layer thicknesses were approximated from the 50 % intensity values in the normalized depth profiles and indicate Ba depletion layers in the range of 10–120 nm, varying as a strong function of poling voltage ($\propto V^2$). The layer thickness data for both layers are summarized in Fig. 5 and show a quadratic dependence with respect to poling voltage. This

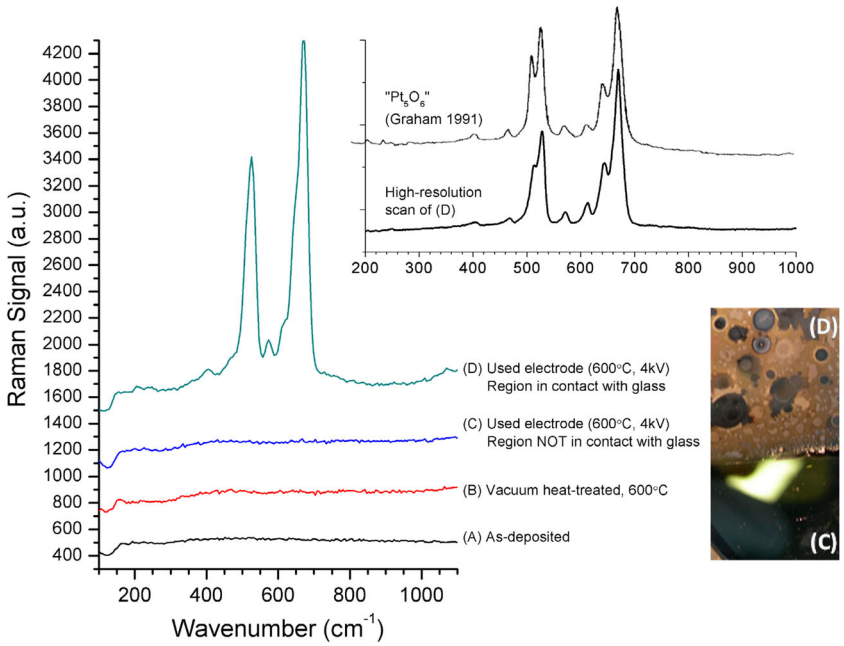

Fig. 3 Raman spectra of surface of Pt film electrode surfaces (*A*) as-deposited, (*B*) vacuum heat-treated at 600 °C for 1 h, and (*C*, *D*) after use as press-contact electrode for poling at 600 °C, where (**c**) is a region held at high voltage but not in contact with the glass [see image] and (**d**) is in the poled/corroded region in contact with the glass. *(Inset)* High-resolution scan of the spectrum in (d), identifying the phase as Pt_5O_6 [43]

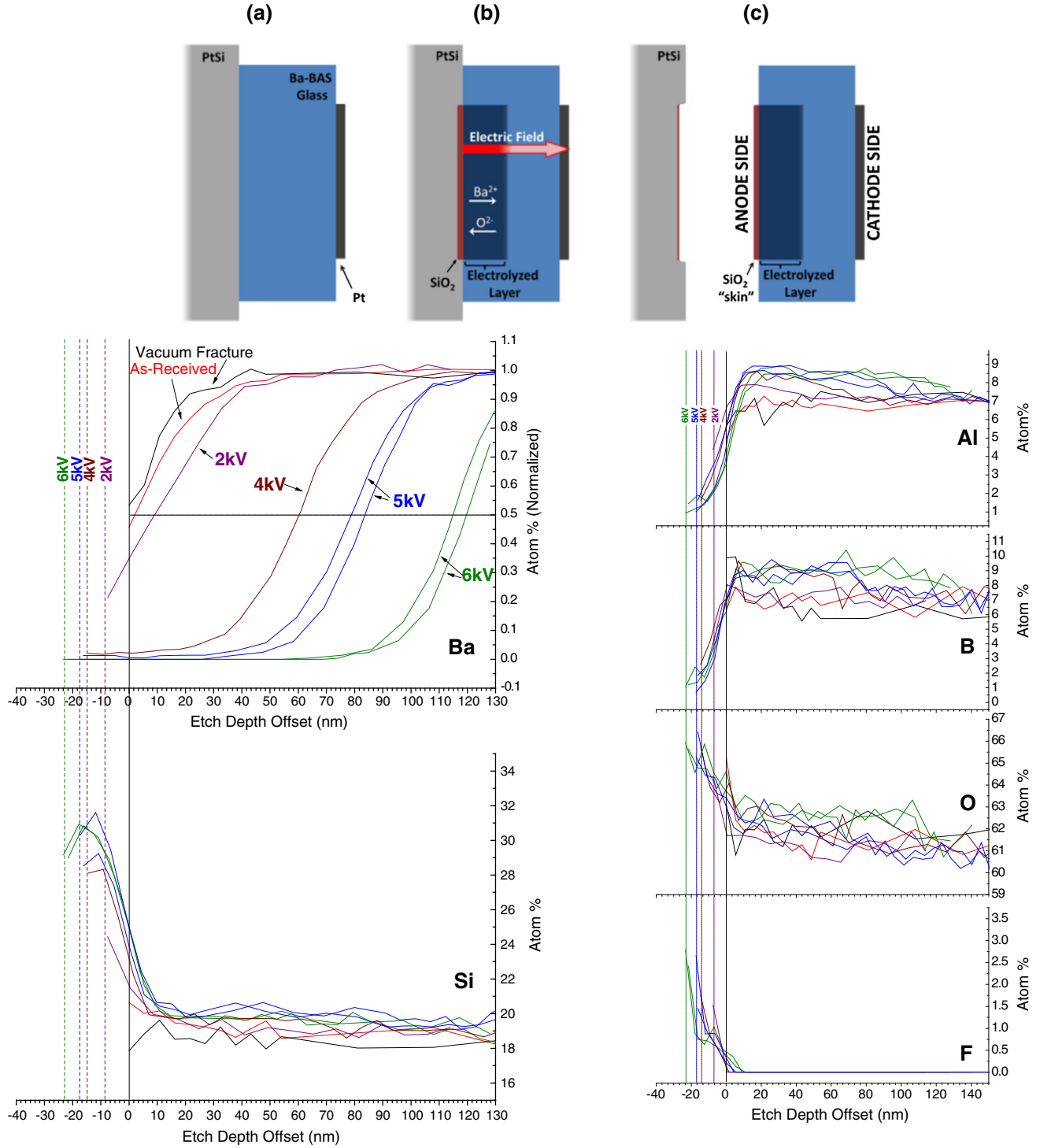

Fig. 4 *(upper)* Schematic depiction of anodic oxidation during poling with PtSi electrode, where in a SiO_2-rich interfacial oxide is formed and subsequently detaches with the glass during separation from the electrode within the poled region of the anode-side glass surface. *(lower)* XPS sputter depth profiles of poled glass surfaces (anode side), poled with PtSi anodes, at varying applied voltages (60 °C, 30 min.). In the depth profiles, the approximate thickness of the SiO_2 skin was estimated from the depth at 50 % of the peak value and was in the range of 5–20 nm. The estimated thickness values were used to offset the depth profiles for the remaining elements in the glass, effectively aligning the "original glass surface" at zero

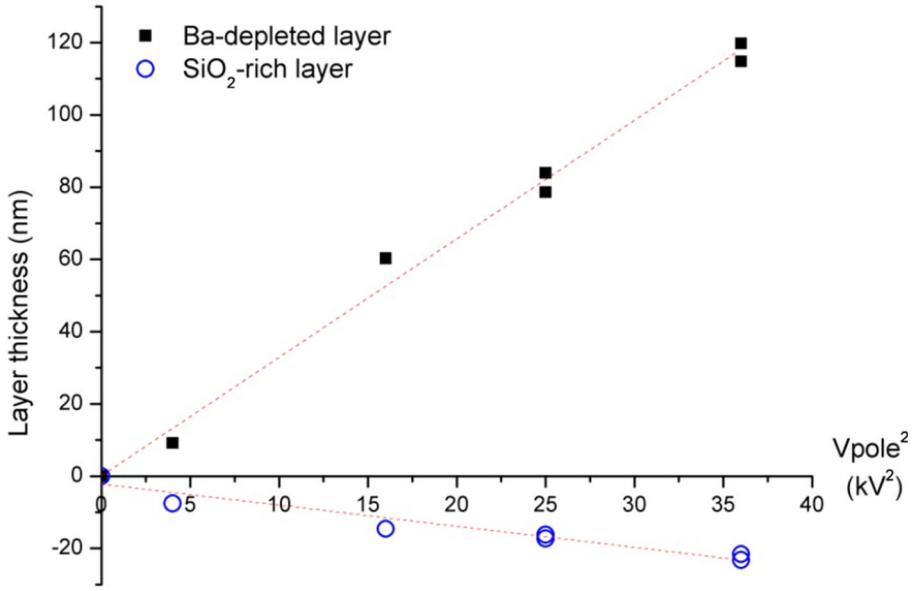

Fig. 5 Quadratic dependence of layer thickness with poling voltage using PtSi electrodes (600 °C, 30 min; thickness estimated from XPS depth profiles, as described in the text)

supports the idea of oxygen and barium counter-migration driven by the electric field distribution within the glass, but the strong dependence on electrode material indicates a more complex interplay with oxidation at the anode as a factor in determining layer thickness.

Another important consideration in the formation of the depletion layers is the role of cations like H^+/H_3O^+. Such species can serve to charge compensate the structure in the absence of virtually all other modifiers and could arise from either injection at the anode surface, or perhaps even from the electrolysis of bulk water within the glass structure [10]. The bulk water content in this glass was measured at approximately 1,400 ppm-mol H_2O based on infrared transmission measurements and the practical extinction coefficient reported by Illievski [44].

To address this aspect, we summarize in Fig. 6 the SIMS depth profile results for both the unpoled control and the poled anode-side surface of the glass sample. The poled sample in this case was chosen to produce a relatively thick, ~60 nm modifier-depleted layer (PtSi electrode, 600 °C, 4 kV), albeit with the added complication of the adherent thin SiO_2-rich "skin" as shown in Fig. 4. The profiles in Fig. 6 for Ba, Al, B, Si and O corroborate the XPS findings already presented. Meanwhile, the H profiles in the inset show that both as-received and poled samples possess a maximum in concentration of H at the outermost surface, likely attributable to water adsorbed on the samples. At the deepest points in the profiles, a steady-state value of ~2,000–3,000 ppm-atom H is found in both poled and control samples. This level agrees well with the bulk water content determined from IR absorbance (1,400 ppm-mol $H_2O \rightarrow$ ~2,800 ppm-atom H as OH^-), cross-validating the SIMS quantification. After poling, there is a discernible subsurface peak in the profile suggesting an "excess" of H within the surface layer. To provide a better quantitative account of this feature, Fig. 6 also shows the difference profile for the hydrogen, ΔH, by elimination of the hydrogen background. The ΔH profile for the poled glass surface shows little correlation with the Ba-depleted layer, where Ba^{2+} is reduced by ~1 order of magnitude to a depth ~60–70 nm. Thus, it is unlikely that water reaction or proton exchange is responsible for charge compensation through the Ba^{2+} depleted layer. In fact, it would require 7 atom % H^+ to compensate the Ba^{2+} in this layer (i.e., two times the original Ba concentration of 3.5 atom %). This confirms, again, the role of oxygen anion counter-diffusion and an associated change in the glass structure within the modifier depleted layer to provide for charge neutrality (see next section). The small 1.5 % accumulation of H at the outermost region of the Ba depleted layer is likely due to adsorbed water trapped or injected at the original electrode–glass interface, as observed in several other studies with poling phenomena.

3.2 Characterization of the depletion layer structure and properties

In this section, FTIR spectroscopy is used to evaluate the nature and magnitude of structural alteration within the poled depletion layers. It is important to keep in mind that these modified layers are "optically thin" with respect to the information depth of infrared measurements—typically considered as 0.5–2 μm depending on the absorptivity at a given wavelength—and so there is some convolution of the spectra for the surface layer with the underlying bulk glass To help maximize signal representative of the poled

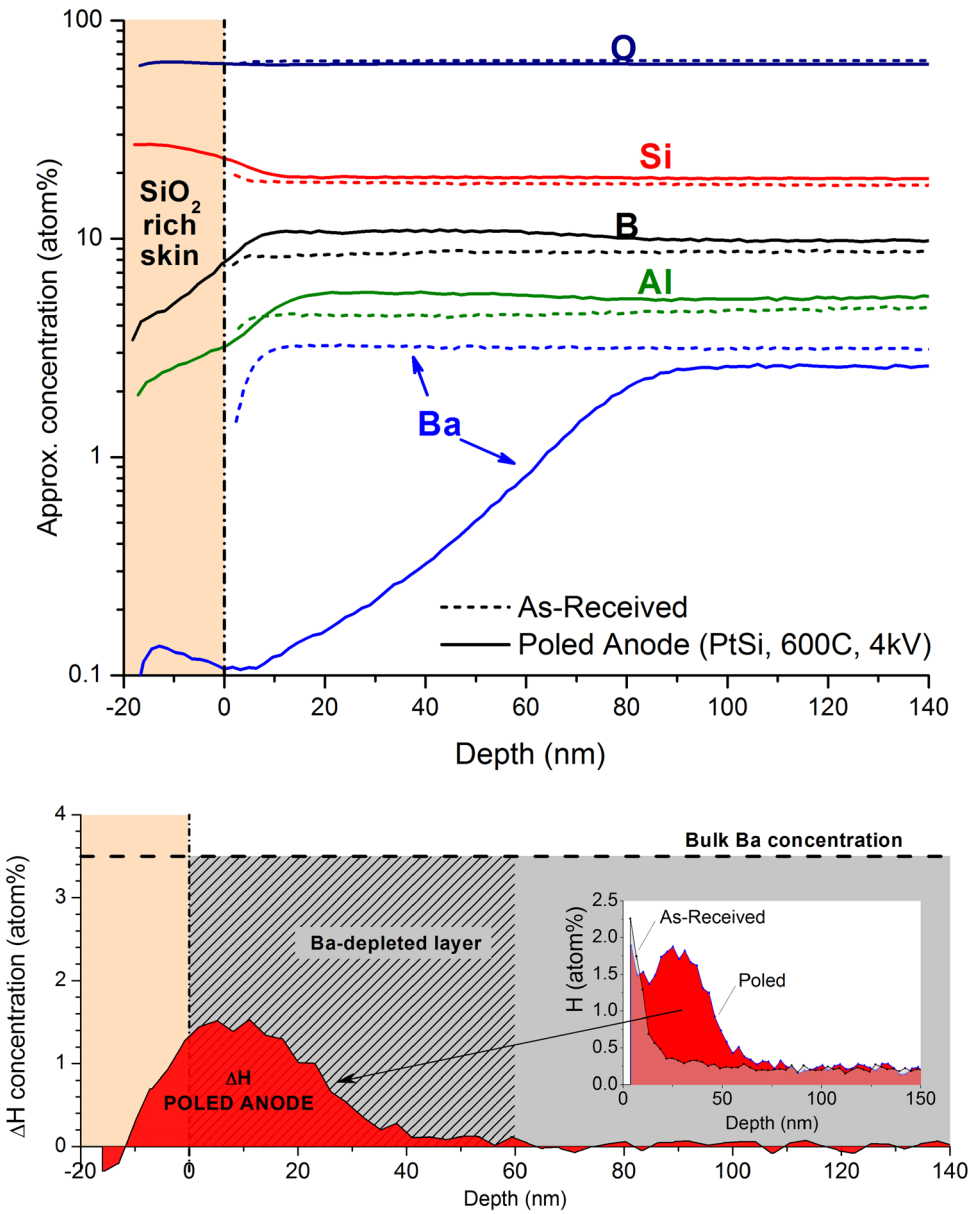

Fig. 6 *(top)* SIMS depth profile of the poled anode-side glass surface (PtSi electrode, 600 °C, 4 kV, 30 min.), compared to as-received control (*dotted line*), with profiles offset to approximately align original glass surfaces in the absence of SiO_2 skin (see text). *(bottom)* The inset shows the overlaid H profiles without the depth offset, highlighting background contributions attributed to surface hydration and bulk water content. The difference profile (ΔH) is shown by subtracting these contributions

surface layers, we focus on glasses poled with PtSi electrodes at 600 °C, as these samples possess the thickest modified layers and, therefore, offered the greatest opportunity to differentiate the layer structure from the bulk glass. It is also to be noted that the samples are designated by their respective poling voltage, although they could be equally designated by their depleted layer thickness (see Fig. 5).

Figure 7 presents the normalized infrared reflectance spectra for the as-received glass along with those for the anode- and cathode-side surfaces of the poled glass samples at various voltages. This mid-IR spectral region contains a number of strong absorption bands associated with the glass network structure. In the as-received glass, the peak structure in the range of 1,300–1,500 cm^{-1} is generally assigned to O–B–O stretches for boron associated with the silicate network. At lower wavenumber, a large, broad reflectance signal from 1,000 to 1,100 cm^{-1} is observed, with its peak at ~1,075 cm^{-1} and a shoulder on the low wavenumber side. Peaks at these frequencies are generally ascribed to symmetric and asymmetric stretches of bridged tetrahedral units for Si, B or Al oxides [36, 45, 46]. The shoulder on the low wavenumber side is attributed to modifier species associated with the network tetrahedra, most commonly non-bridging Q^n species on silica tetrahedra, or the anionic $[AlO_4]$ and $[BO_4]$ tetrahedral units that are present in this glass. Of course, a rigorous interpretation of reflection spectra, especially for this case of a layered sample, requires significant data treatment [47, 48]. But based on the significant literature, it is possible to

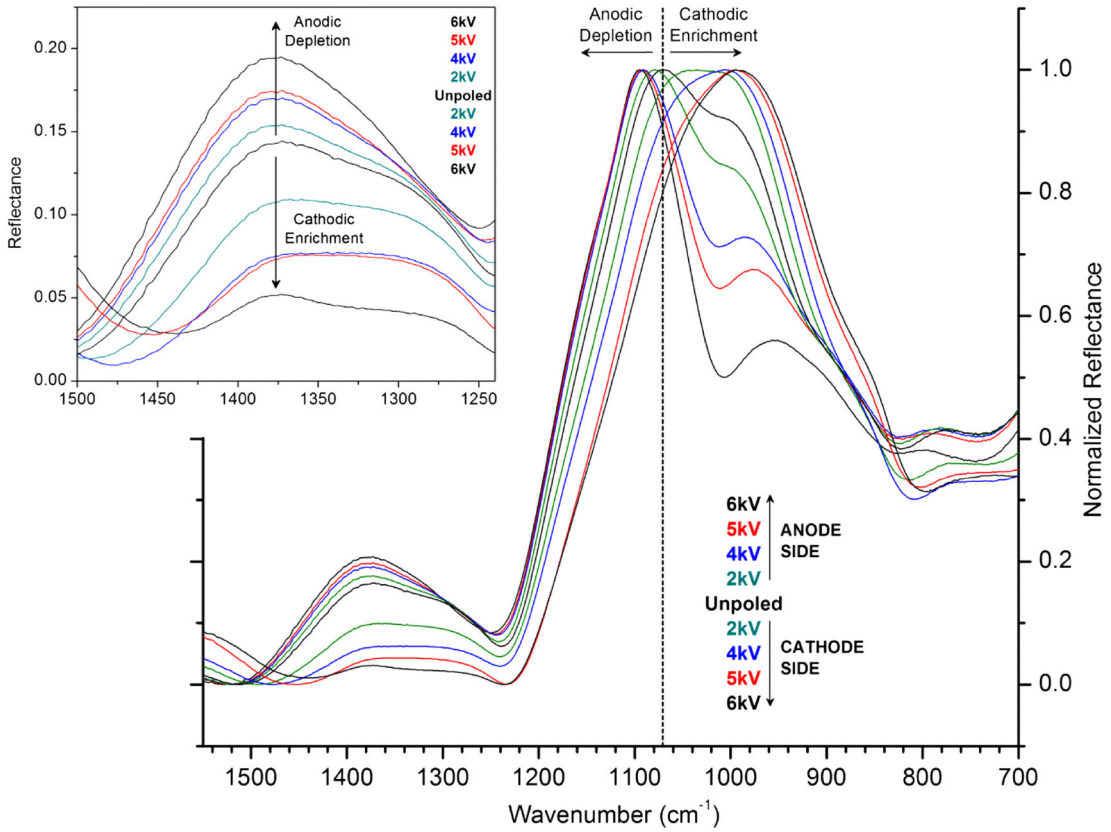

Fig. 7 Changes in normalized infrared reflectance spectra for anode-side surface—where modifier is strongly depleted—versus cathode-side surface—where modifiers Ba and Na are strongly enriched. *(Inset)* Magnified view of reflectance data in the 1,500–1,250 cm^{-1} range associated with B–O stretches

qualitatively interpret changes in the IRRS spectra directly, as described below.

Figure 7 indicates a pronounced change in the IR spectra at the anodic surface due to the poling process. Most evident in the spectra is a shift to higher wavenumber and sharpening of the primary absorption peak in the 1,000–1,150 cm^{-1} range, along with a deepening separation and a more distinct shoulder/peak on the low wavenumber side. Qualitatively, these spectral changes resemble those observed in the IR reflectance spectra of leached surface layers, where—as the surface composition becomes modifier-depleted and SiO_2-rich—the Si–O spectral signatures for the surface layer shift and sharpen to resemble those of the fully polymerized network of fused silica ($\sim$1,122 cm^{-1}), while the low wavenumber shoulder decouples reflecting its origin in the underlying bulk. On the cathodic surface, an opposing trend is observed, wherein the primary stretching peak broadens and shifts to lower wavenumber due to incorporation of new lower frequency modes. These spectral changes are consistent with the accumulation/incorporation of excess modifier (Ba, Na) into the glass network. The creation of NBO or [BO_4] to accommodate the additional modifier would require additional oxygen or more complex borate or aluminate structures, or alternatively the formation of zero-valent Ba. There was no evidence for zero-valent Ba in the XPS data for the cathode-side surface, and so changes in the local structure for B and Al must be considered.

In the case of boron, the high-frequency B–O stretching vibrations between 1,500 and 1,250 cm^{-1} can provide information about structure changes due to poling. In the as-received glass, the vibrational spectra is clearly composed of at least two B–O components, with a peak located at $\sim$1,373 cm^{-1} and a shoulder at $\sim$1,290 cm^{-1}. The identification of these peaks is based on IR spectral studies of alkaline-earth borates, alkaline-earth aluminoborates and a series of analogous barium-boroaluminosilicates [29, 36, 49–51]. Accordingly, these stretching vibrations are assigned to trigonal B–O and the B-NBO stretching vibrations in [BO_3] units. With the increasing influence of the poled layer on the anode surface, there is a substantial change in the ratio of the two components, with the higher frequency component becoming increasingly prominent and the latter component remaining almost constant. This signifies an increase in concentration of [BO_3] due to Ba depletion on the anode-side depleted surface layer. On the

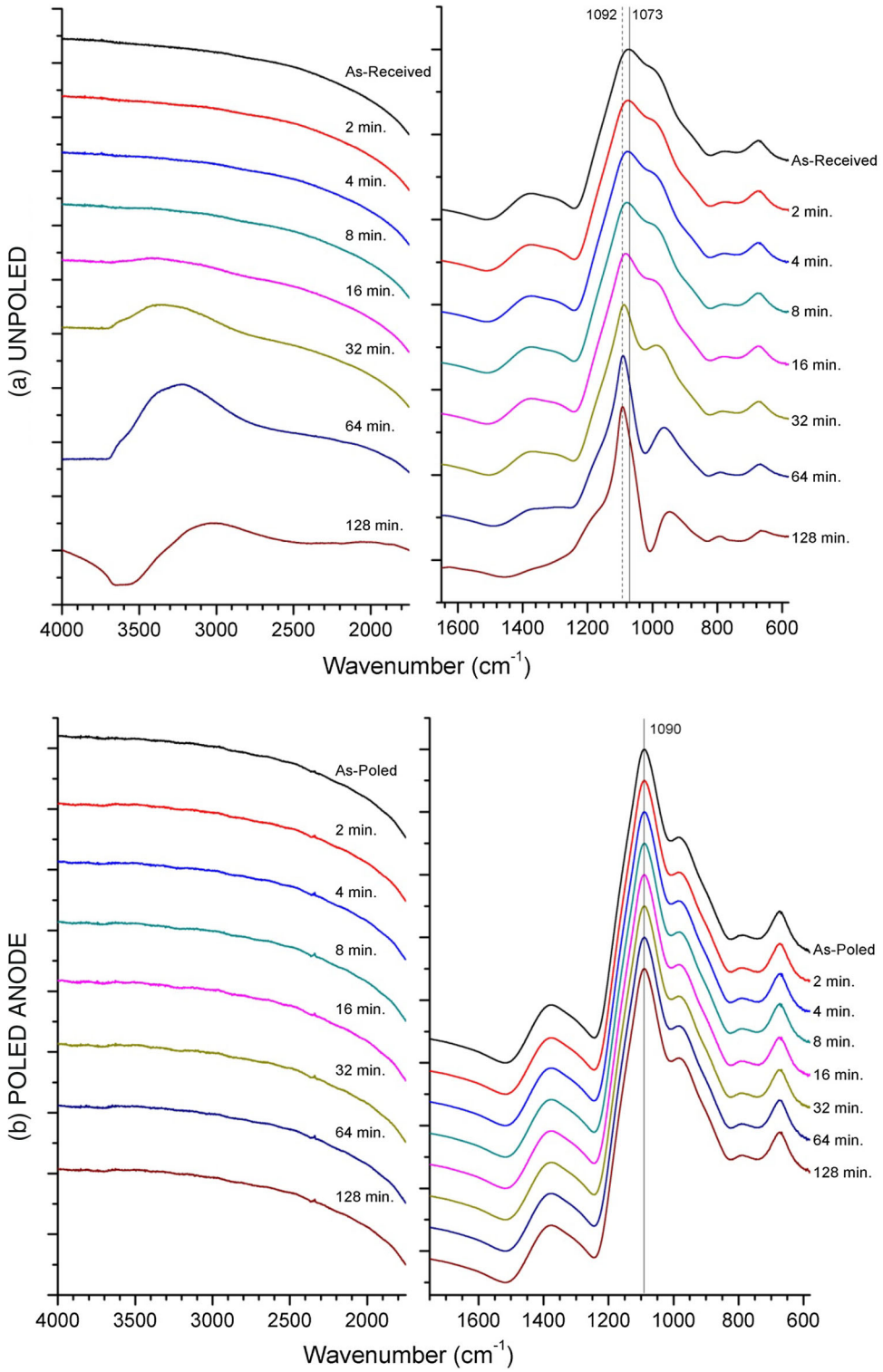

Fig. 8 Evolution of infrared reflectance spectra for AF45 glass leached in warm aqua regia for various durations. (**a**) unpoled, versus (**b**) poled anode surface (4 kV, 600 °C, PtSi anode)

cathodic-side surface, the B–O peak structure shows the opposite trend suggesting an increase in the relative concentration of B-NBO due to the accumulation of excess Ba modifier. Unfortunately, the $[BO_4]$ units vibrate at lower frequencies (800–1,150 cm^{-1}) where there is overlap with the other tetrahedral network units $[SiO_4]$ and $[AlO_4]$ [36]; thus, direct information about changes in $[SiO_4]$ and $[AlO_4]$ due to poling is not evident in the IRRS spectra. Clearly, these FTIRRS results do not explain all of the structural changes required to account for the changes in composition

on the anode- and cathode-side surfaces, but they are consistent with the glass structure models already described. In a companion paper, NMR and Al K-edge XANES are used to further characterize structure changes associated with Al in the network.

Considering the structure changes described above, especially on the anode-side surface, we now use a leaching experiment to further characterize and confirm the effects of high-temperature thermal poling. The glass samples were immersed in a warm solution of strong acid (aqua regia, $1HNO_3$:4HCl:$5H_2O$) at 45 °C for increasing durations of time, and the FTIRRS spectra were measured at intervals proportional to time$^{1/2}$. Fig. 8a shows the results obtained for the as-received/unpoled glass. A main feature of these spectra is the shift of the primary Si–O stretching peak to higher frequency with a deepening valley on the low-frequency side, similar to spectra for the modifier-depleted anode layer of poled glass. However, the B–O stretches in the 1,250–1,500 cm^{-1} region diminish significantly in height during leaching, commensurate with extraction of boron from the silicate network in acid (whereas boron is not removed during poling). In the high-frequency region, the leached samples present significant OH absorption bands in the 3,500–3,300 cm^{-1} region, indicating the strong uptake of H^+/H_3O^+ in the structure in exchange for the leached modifier species (Ba^{2+}). These observations confirm that poling-induced depletion layers are structurally dissimilar from leached/ion-exchanged layers in their H content and provide further evidence that alternate mechanisms—such as anion migration—occur to accommodate the loss of modifier.

In Fig. 8b, we show a series of spectra for a poled anode-side surface (4 kV) after the acid treatment. It is evident that the spectra are virtually unchanged for the entire duration of the study, with only a slightly detectable increase in the 3,575 cm^{-1} OH stretching region after 1–2 h of exposure. Compared to the unpoled glass, the very limited ingress of H^+/H_3O^+ in the strong acid solution is consistent with the reduced possibility for ion-exchange in the Ba modifier depleted network, as well as reduced extraction of (typically acid-extractable) boron and aluminum from the poled layer. These results are thus consistent with a poling-induced structural transformation in the depleted layer which yields a stable boroaluminosilicate network not readily penetrated, leached or dissolved by the aqueous acid solution.

4 Discussion

In thermal poling for SON, it is the violation of local charge-neutrality by cations drifting away from the vicinity of "immobile" anions which provides the basis for inducing a static DC field and thereby creating second-order nonlinearity, $\chi^{(2)}$. Fortunately, it requires a very minor concentration of migrated charges—of the order of ppm—to achieve the electric field and $\chi^{(2)}$ magnitudes commonly observed in poled glass. At the higher poling temperatures used here, where $\chi^{(2)}$ is observed to diminish, it is difficult to sustain the charge separation. For this particular glass, a $\chi^{(2)}$ susceptibility of 0.26 pm/V was determined at 600 °C with the Pt film electrodes (see Fig. 2), with a corresponding internal field of $\sim$2.2 MV/cm per the rectification model of poling-induced SON (see [20]). Even in the case where the SON is due solely to Ba migration and localized to the 60 nm Ba-depletion layer, it can be subsequently estimated that only 1.2×10^{18} elementary charges/cm^3 would need to be displaced to achieve the calculated field. This corresponds to only $\sim$0.16 % of the charge deficit created by all of the Ba-ion depletion observed at 600 °C. This is further evidence, independent of the spectroscopy that some mechanism of charge compensation has occurred through structural modification of the glass network in the depleted layer. Related to this point, it was also shown by several methods that the injection of protonated H^+/H_3O^+ species at the anode was successfully mitigated by our process methodology. If we assume that the ΔH profile (see Fig. 6) is all present as H^+, integration of the ΔH profile indicates its drift into the glass can only account for $\sim$10 % of the total charge deficit from Ba^{2+}. Thus, the presence of protonated species in the poled anode layer—while not zero—is also insufficient to account for the structural charge requirements in the depletion layer. This fact also differentiates the structure of these poling-induced depletion layers from those formed by leaching, as exemplified in Figs. 7, 8. These analyses, together with the results already presented, provide a strong case for "electrolysis" of the glass network itself, wherein the counter-migration of anions (O^-, F^-) from with the structure serve to alleviate the substantial excess of negative charge that would otherwise be present in the surface layer.

Accepting this electrolytic mechanism, the question now arises: how does the atomic structure within the glassy depletion layer transform as oxygen and fluorine anions are extracted from the parent glass network? It may be recalled that BaO in the initial glass structure is allocated primarily to charge-compensating $[TO_4]^-$ tetrahedra in the structure rather than to the creation of non-bridging oxygen (NBO). The results of ^{27}Al MAS-NMR for the bulk glass—presented in a separate report [37]—corroborate this allocation, where the vast majority ($\sim$95 %) of the aluminum is present as Al[4] and would require charge-compensation from Ba^{2+} ions—about 73 % of the total Ba content. The remaining Ba then enters the structure by converting B[3] $\rightarrow$ B[4], with NBO being a very limited, minority species. Thus, the

relevant anionic species that must be considered for the electrolytic extraction of oxygen are $[AlO_4]^-$, as well as some $[BO_4]^-$ and, as yet, unknown fluorine species. One straightforward mechanism for the structural transition is conversion of boron from the tetrahedral state to a charge-neutral, 3-coordinated trigonal state. This follows from classical concepts of the so-called boron anomaly. The conversion may be represented with the following reaction:

$$Ba^{2+} + 2\left[BO_{4/2}\right]^- \rightarrow Ba^{2+}\left(\uparrow_{cathode}\right) + O^{2-}\left(\downarrow^{anode}\right) + 2\left[BO_{3/2}\right]$$

yielding two $[BO_3]$ units per O^{2-} anion. In the current study, evidence for the B[4] → B[3] reaction is inferred from the systematic changes in the B–O stretching region of the IR spectra related to $[BO_3]$ units and analogous to the IR spectral studies of boroaluminosilicate glasses. In comparing the IR spectra for both the anode- and cathode-side surface layers, the "parent" network becomes, respectively, depleted and enriched with modifier, and the observed intensity correlation in both directions is suggestive of this same conversion reaction. An identical mechanism of B[4] → B[3] conversion has been implicated in electrolyzed alkali borates [14, 15]. A similar approach is applied to investigate the Al environment within the poled depletion layer, the details of which are described in a separate report using XANES/NEXAFS [38, 52–54].

5 Summary

The results of this work provide insight into the mechanisms of structural and compositional modifications that occur in the anodic layer of an alkali-free multicomponent glass system during thermal poling. In this work, the goal was not to optimize poling for second-order nonlinearity, but rather to understand the associated composition and structure changes over a wider range of poling conditions. We have established conditions for thermal poling of this glass to induce a Ba^{2+}/Na^+-depleted layer on the anodic surface, mostly free of H^+ or other cation injection, and through which the structure achieves charge-compensation mainly by counter-migration of anionic (O^{2-}/F^-) species from within the glass network. This process is non-spontaneous—being activated by temperature and voltage—and is observed to be strongly dependent on the nature of the electrode interface. This model necessarily implies significant modification of the atomic structure within the poled layer on the anode side surface. Using a variety of direct analytical methods applied to the electrode and glass surfaces, it was found that the resultant layer composition is composed of essentially only the network-forming species, B_2O_3-Al_2O_3-SiO_2. This extremely network-former-rich composition synthesized near the surface would be expected to exhibit dramatically different properties from the bulk glass. The data presented show indications of such altered properties in both (1) a reduction in refractive index, with an anti-reflection effect tunable with poling-voltage/layer-thickness, and (2) a substantially improved hydrolytic resistance of the glass surface at low-pH, consistent with the elimination of modifier from the surface (thereby mitigating the mechanism of H^+/H_3O^+-for-RO ion-exchange) and the limited ingress of water consistent with a re-polymerized network structure at the surface.

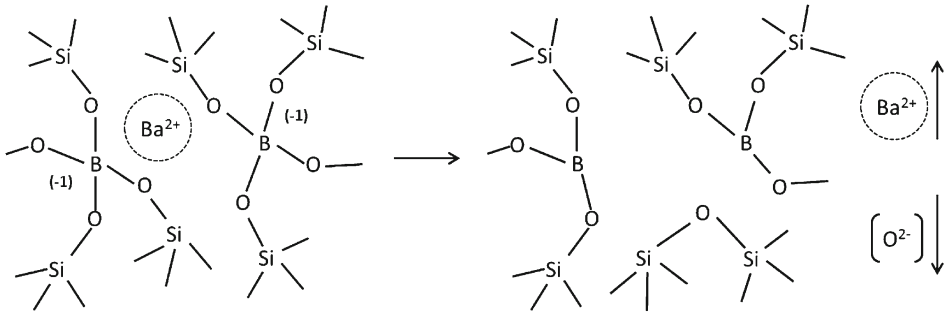

Acknowledgments The authors acknowledge The Office of Naval Research under Grant N00014-05-1-0541 and the Penn State Materials Research Institute for partial funding of this work. The authors also thank Vince Bojan and Josh Stapleton (Penn State University) for their help and guidance regarding materials analysis throughout this work.

References

1. M. Dussauze et al., Thermal poling of optical glasses: mechanisms and second-order optical properties. Int. J. Appl. Glass Sci. **3**(4), 309–320 (2012)
2. S. Fleming, H. An, Progress in creating second-order optical nonlinearity in silicate glasses and waveguides through thermal poling. Front Optoelectron. China **3**(1), 84–91 (2010)

3. M. Dussauze et al., Polarization mechanisms and structural rearrangements in thermally poled sodium-alumino phosphate glasses. J. Appl. Phys. **107**(4), 043505 (2010). 1-043505/6
4. M. Dussauze et al., How does thermal poling affect the structure of soda-lime glass? J. Phys. Chem. C **114**(29), 12754–12759 (2010)
5. D. Moncke et al., Thermal poling induced structural changes in sodium borosilicate glasses. Phys. Chem. Glasses Eur. J. Glass Sci. Technol. Part B **50**(3), 229–235 (2009)
6. M. Dussauze et al., Structural rearrangements and second-order optical response in the space charge layer of thermally poled sodium niobium borophosphate glasses. J. Phys. Chem. C **111**(39), 14560–14566 (2007)
7. D.E. Carlson, K.W. Hang, G.F. Stockdale, Ion depletion of glass at a blocking anode: II, properties of ion-depleted glasses. J. Am. Ceram. Soc. **57**(7), 295–300 (1974)
8. D.E. Carlson, Ion depletion of glass at a blocking anode: I, theory and experimental results for alkali silicate glasses. J. Am. Ceram. Soc. **57**(7), 291–294 (1974)
9. E.C. Ziemath, V.D. Araujo, J.C.A. Escanhoela, Compositional and structural changes at the anodic surface of thermally poled soda-lime float glass. J. Appl. Phys. **104**(5), 054912–054917 (2008)
10. K.P. Gadkaree et al., Single-crystal silicon films on glass. J. Mater. Res. **22**(9), 2363–2367 (2007)
11. K.B. Albaugh, Irreversibility of anodic bonding. Mater. Lett. **4**(11–12), 465–469 (1986)
12. D.E. Carlson, K.W. Hang, G.F. Stockdale, Electrode "polarization" in alkali-containing glasses. J. Am. Ceram. Soc. **55**(7), 337–341 (1972)
13. T. Cremoux et al., Trapped molecular and ionic species in poled borosilicate glasses: toward a rationalized description of thermal poling in glasses. J. Phys. Chem. C. **118**(7), 3716–3723 (2014)
14. Baucke, F.G.K. and J.A. Duffy, Electrolysis of a sodium borate glass: a new mechanism of oxide ion transport. Glastechnische Berichte 56(Int. Glaskongr., 13th, Band 1): 608–613 (1983)
15. F.G.K. Baucke, J.A. Duffy, Ion migration study in a sodium borate glass: proposal of a new oxide transport. J. Electrochem. Soc. **127**(10), 2230–2233 (1980)
16. B. Schmidt et al., In situ investigation of ion drift processes in glass during anodic bonding. Sens. Actuators A **67**(1–3), 191–198 (1998)
17. A.T.J. van Helvoort et al., Anodic oxidation during electrostatic bonding. Philos. Mag. **84**(6), 505–519 (2004)
18. A.T.J. van Helvoort, K.M. Knowles, J.A. Fernie, Characterization of cation depletion in pyrex during electrostatic bonding. J. Electrochem. Soc. **150**(10), G624–G629 (2003)
19. K.B. Albaugh, D.H. Rasmussen, Rate processes during anodic bonding. J. Am. Ceram. Soc. **75**(10), 2644–2648 (1992)
20. N.J. Smith, M.T. Lanagan, C.G. Pantano, Thermal poling of alkaline earth boroaluminosilicate glasses with intrinsically high dielectric breakdown strength. J. Appl. Phys. **111**(8), 083519-9 (2012)
21. A. Ellison, I.A. Cornejo, Glass substrates for liquid crystal displays. Int. J. Appl. Glass Sci. **1**(1), 87–103 (2010)
22. N.J. Smith et al., Alkali-free glass as a high energy density dielectric material. Mater. Lett. **63**(15), 1245–1248 (2009)
23. H. Lee et al., Dielectric breakdown of thinned $BaO–Al_2O_3–B_2O_3–SiO_2$ glass. J. Am. Ceram. Soc. **93**(8), 2346–2351 (2010)
24. P. Dash et al., Activation energy for alkaline-earth ion transport in low alkali aluminoborosilicate glasses. Appl. Phys. Lett. **102**(8), 082904–082905 (2013)
25. T. Murata et al., Electrode-limited dielectric breakdown of alkali free glass. J. Am. Ceram. Soc. **95**(6), 1915–1919 (2012)
26. E. Furman, High temperature performance of coiled glass capacitors. Presented at HiTEC 2012, International Microelectronics Assembly and Packaging Society (2012)
27. A.E. Owen, Properties of glasses in the system CaO-B2O3-Al2O3. Part. 1. The d. c conductivity and structure of calcium boroaluminate glasses. Phys. Chem. Glasses **2**(3), 87–98 (1961)
28. S. G. Bishop, P. J. Bray, NMR studies of Ca boroaluminate glasses. Phys. Chem. Glasses 7(3) (1966)
29. M. T. Strzelecki, The corrosion behavior of barium aluminoborosilicate glass and its relation to glass structure. thesis in MatSE p. 132 (1999)
30. J.G. Wood et al., The effects of antimony oxide on the structure of alkaline-earth alumino borosilicate glasses. J. Non Cryst. Solids **349**, 276–284 (2004)
31. Q. Zheng et al., Composition–structure–property relationships in boroaluminosilicate glasses. J. Non Cryst. Solids **358**(6–7), 993–1002 (2012)
32. I.D. Tykachinskii et al., The coordination of boron and aluminum in some barium aluminosilicate glasses. J. Appl. Spectrosc. **13**(6), 1660–1661 (1970)
33. L.-S. Du, J.F. Stebbins, Network connectivity in aluminoborosilicate glasses: a high-resolution 11B, 27Al and 17O NMR study. J. Non Cryst. Solids **351**(43–45), 3508–3520 (2005)
34. W.J. Dell, P.J. Bray, S.Z. Xiao, 11B NMR studies and structural modeling of Na2O—B2O3—SiO2 glasses of high soda content. J. Non Cryst. Solids **58**(1), 1–16 (1983)
35. H. Yamashita et al., Nuclear magnetic resonance studies of 0.139MO (or M'2O) and #xB7; 0.673SiO2 and #xB7; (0.188-x)Al2O3 and #xB7; xB2O3 (M = Mg, Ca, Sr and Ba, M' = Na and K) glasses. J. Non Cryst. Solids **331**(1–3), 128–136 (2003)
36. Y.D. Yiannopoulos, E.I. G. D. K. Chryssikos, Structure and properties of alkaline earth borate glasses. Phys. Chem. Glasses **42**, 164–172 (2001)
37. S. Sen et al., Atomic-scale understanding of structural relaxation in simple and complex borosilicate glasses. Phys. Rev. B **75**(9), 094203 (2007)
38. N. Smith, C. Pantano, T. Regier, Manuscript in preparation
39. N.J. Smith, Novel approaches to the surface modification of glass by thermal poling. Ph.D. thesis in Mater. Sci. Engr. p. 190 (2011)
40. G.C. Smith, Evaluation of a simple correction for the hydrocarbon contamination layer in quantitative surface analysis by XPS. J. Electron Spectrosc. Relat. Phenom. **148**(1), 21–28 (2005)
41. C.W. Magee, E.M. Botnick, Hydrogen depth profiling using SIMS—problems and their solutions. J. Vac. Sci. Technol. **19**(1), 47–52 (1981)
42. M.M. Smedskjaer et al., Modifying glass surfaces via internal diffusion. J. Non Cryst. Solids **356**(6–8), 290–298 (2010)
43. G.W. Graham et al., Raman investigation of simple and complex oxides of platinum. J. Raman Spectrosc. **22**(1), 1–9 (1991)
44. S. Illievski et al., Practical IR extinction coefficients for water in commercial glasses determined by nuclear reaction analysis. Glass Sci. Technol. **73**(2), 39–45 (2000)
45. P. McMillan, B. Piriou, The structures and vibrational spectra of crystals and glasses in the silica-alumina system. J. Non Cryst. Solids **53**(3), 279–298 (1982)
46. B.O. Mysen, P. Richet, *Silicate glasses and melts: properties and structure*, 1st edn., Developments in geochemistry (Elsevier, Boston, 2005), p. 544
47. F. Geotti-Bianchini et al., New interpretation of the IR reflectance spectra of silica-rich films on soda-lime glass. Glastechnische Berichte **64**(8), 205–217 (1991)
48. S.A. MacDonald et al., Dispersion analysis of FTIR reflection measurements in silicate glasses. J. Non Cryst. Solids **275**(1–2), 72–82 (2000)
49. E.I. Kamitsos, G.D. Chryssikos, M.A. Karakassides, New insights into the structure of alkali borate glasses. J. Non Cryst. Solids **123**(1–3), 283–285 (1990)
50. K. El-Egili, Infrared studies of Na2O-B2O3-SiO2 and Al2O3-Na2O-B2O3-SiO2 glasses. Phys. B **325**, 340–348 (2003)

51. I. Polyakova et al., Application of the constant stoichiometry grouping concept to the Raman spectra of BaOAl2O3B2O3 glasses. Phys. Chem. Glasses Eur. J. Glass Sci. Technol. Part B **51**, 52–58 (2010)
52. U.K. Krieger, W.A. Lanford, Field assisted transport of Na+ ions, Ca2+ ions and electrons in commercial soda-lime glass I: experimental. J. Non Cryst. Solids **102**(1–3), 50–61 (1988)
53. R.A Schaut, The effect of boron oxide on the composition, structure, and adsorptivity of glass surfaces. Ph.D. thesis in MatSE (2008)
54. M.E. Fleet, S. Muthupari, Boron K-edge XANES of borate and borosilicate minerals. Am. Mineral. **85**(7–8), 1009–1021 (2000)